ACS APPLIED MATERIALS & INTERFACES

Research Article

www.acsami.org

Fabrication of a Biomass-Based Hydrous Zirconium Oxide Nanocomposite for Preferable Phosphate Removal and Recovery

Hui Qiu,*[,†] Chen Liang,[†] Xiaolin Zhang,*[,‡] Mindong Chen,[†] Yunxia Zhao,[†] Tao Tao,[†] Zhengwen Xu,[†] and Gang Liu[†]

[†]Jiangsu Key Laboratory of Atmospheric Environment Monitoring and Pollution Control, Collaborative Innovation Center of Atmospheric Environment and Equipment Technology, School of Environmental Science and Engineering, Nanjing University of Information Science & Technology, Nanjing 210044, People's Republic of China

[‡]State Key Laboratory of Pollution Control and Resource Reuse, School of the Environment, Nanjing University, Nanjing 210093, People's Republic of China

Supporting Information

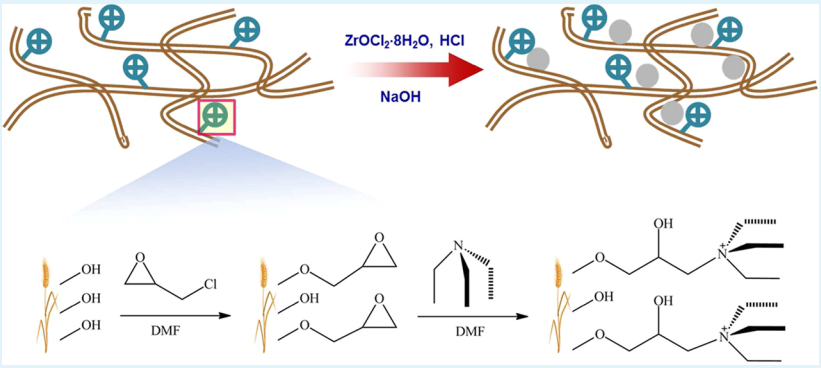

ABSTRACT: Advanced removal of phosphate by low-cost adsorbents from municipal wastewater or industrial effluents is an effective and economic way to prevent the occurrence of eutrophication. Here, we proposed a novel method to immobilize hydrous zirconium oxide nanoparticle within quaternary-aminated wheat straw, and obtained an inexpensive, eco-friendly nanocomposite Ws−N−Zr. The biomass-based Ws−N−Zr exhibited higher preference toward phosphate than commercial anion exchanger IRA-900 when competing sulfate ions coexisted at relatively high levels. Such excellent performance of Ws−N−Zr resulted from its specific hybrid structure, the quaternary ammonium groups bonded on the host favor the preconcentration of phosphate ions inside the wheat straw based on Donnan effect, and the encapsulated HZO nanoparticle exhibits preferable sequestration of phosphate ions through specific interaction, as further demonstrated by FTIR and X-ray photoelectron spectroscopy. Cycle adsorption and regeneration experiments demonstrated that Ws−N−Zr could be employed for repeated use without significant capacity loss, when the binary NaOH−NaCl solution was employed as the regenerant. The influence of solution pH and contact time was also examined. The results suggested that Ws−N−Zr has a great potential in efficient removal of phosphate in contaminated waters.

KEYWORDS: *biomass, hydrous zirconium oxide, phosphate, nanocomposite, FTIR study*

1. INTRODUCTION

Release of phosphorus into groundwater and surface water has already caused serious eutrophication problems on a global scale, which affects the survival of many aquatic species and the safety of drinking water supplies.[1,2] Studies reveal that lake water concentrations of P above 0.02 ppm could generally accelerate eutrophication.[3,4] Thus, enhanced removal of phosphate from waste effluents is of considerable significance before their discharge into the receiving waterways.[5] On the other hand, as a nonrenewable resource, the limited supply of phosphate in the near future makes its recovery from wastewater even more urgent.[6,7] For example, the phosphorus contained in wastewater in UK, if fully recovered, is estimated to meet nearly one-half of the country's fertilizer demand.[8]

The conventional techniques for phosphate removal, such as chemical precipitation, biological removal, and electrochemical treatment, usually cannot meet the increasingly stringent regulation nowadays, or cannot be used as a way for phosphate recycle.[9,10] Adsorption has been regarded as an attractive alternative because of its simple operation, low cost, and potential for phosphate recovery from wastewater.[11,12] Among the available adsorbents, hydrated ferric oxide (HFO) has been extensively studied and widely used in phosphate removal in wastewater or surface waters because of its satisfactory capacity

Received: July 7, 2015
Accepted: September 4, 2015
Published: September 4, 2015

DOI: 10.1021/acsami.5b06098
ACS Appl. Mater. Interfaces 2015, 7, 20835−20844

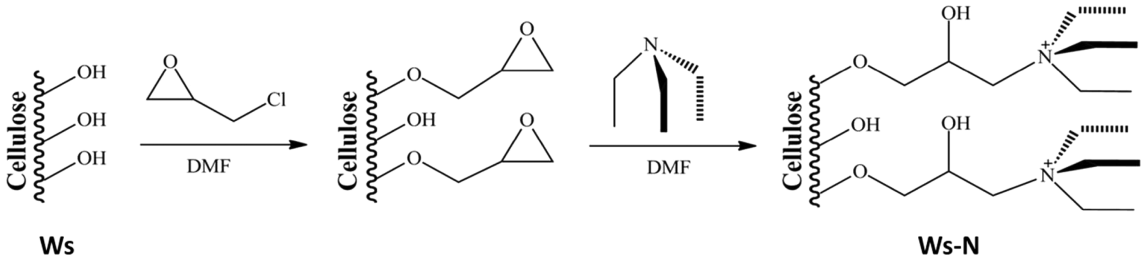

Figure 1. Preparation steps for biomass-based anion-exchanger Ws−N.

and relatively low operation cost. Moreover, HFO exhibits preferable phosphate removal through formation of inner-sphere complexes via Lewis acid−base interactions.[13,14] However, HFO was unstable and feasible to dissolve under acidic conditions. The potential secondary pollution by Fe leaching into waters would exert adverse effects to organisms.[15,16] Similar to HFO, hydrous zirconium oxide could also serve as an efficient adsorbent because it possesses a rich amount of hydroxyl groups and shows high capacity and specific adsorption through Lewis acid−base interaction toward phosphate.[17,18] Unlike HFO, hydrated zirconium oxide (HZO) exhibits high resistance against attacks by acids and bases, organic ligands, and oxidants.[19] Besides, HZO is innocuous, inexpensive, and can be efficiently regenerated by alkaline solution, implying its great potential in decontamination of water from phosphate.[18]

Unfortunately, HZO is usually present as fine or ultrafine particles with the particles size ranging from 20 to 100 nm, which is generally difficult to be directly separated from water and recycled.[20] Loading of HZO on supporters with larger size is an effective approach to overcome these shortcomings, such as activated carbon, zeolite, and ion-exchangers.[21−23] Recently, a polymeric anion exchanger has been demonstrated as a preferable supporter alternative for metal oxides immobilization. For example, Chen et al. impregnated HZO nanoparticles within a strong-base anion-exchanger resin, and the resultant hybrid adsorbent exhibited good removal capacity of phosphate.[23] The immobilized charged ammonium groups bound to the polymeric matrix would enhance permeation and preconcentration of target phosphate within the exchanger phase, which is favorable for its sequestration by the impregnated HZO nanoparticles. However, the synthesis of commercial ion-exchange resin has to use a lot of toxic chemical reagents, such as nitrobenzene, chloromethyl ether, styrene, and divinylbenzene. Moreover, the synthetic techniques of resin are fairly complicated, and usually accompanied by production of toxic byproduct leading to serious secondary pollution to the environment.

Recent research indicated that wheat straw, a common agricultural byproduct consisting of cellulose (32.1%), hemicellulose (29.2%), and lignin (16.4%), could be modified into anion exchangers and replace the commercial ion-exchange resin.[24,25] Cellulose, hemicelluloses, and lignin structures have a large amount of reactive hydroxyl groups that can be easily grafted with various functional polymers. On the basis of that, wheat straw, which is eco-friendly, of low-cost, and widely available, represents a potential alternative as a source of anion exchanger.[26] Besides, the reuse of agricultural byproduct could not only minify the air pollution induced by crop burning, but also facilitate the comprehensive utilization of agricultural residues. In previous research, quaternary ammonium groups were introduced into sugar cane bagasse after reaction with epichlorohydrin and triethylamine in the presence of pyridine as catalyst, and the resulting ion exchanger was applied to adsorb nitrate ions in wastewater.[27,28] However, a serious secondary pollution with large amounts of odoriferous wastewater was produced when using pyridine as catalyst in the preparation. Gao et al. developed a new biomass-based ion exchanger modified by quaternary ammonium groups, using ethlenediamine (EDA) as cross-linking agent to replace pyridine, which showed excellent adsorption properties toward phosphate.[28] Unfortunately, same as the commercial ion exchanger, the absorption of phosphate on biomass-based ion exchangers is mainly based on electrostatic attraction, and the adsorption capacity would significantly decline in the presence of competing anions in water.

In this research, a novel low-cost nanocomposite Ws−N−Zr was developed by immobilizing hydrated zirconium oxide nanoparticle on the inner surface of wheat straw, a typical agricultural byproduct, which has been already modified by quaternary ammonium groups after reaction with epichlorohydrin and triethylamine. The basic morphology and physicochemical properties of the nanocomposite were characterized, and the selective adsorption behavior of phosphate was particularly concerned. Besides the influence of solution pH and adsorption time on adsorption being examined, the underlying adsorption mechanism was further explored with FTIR and X-ray photoelectron spectroscopy. Cyclic adsorption and regeneration experiments were investigated to evaluate the performance and feasibility of the newly developed adsorbent for practical application. A better understanding of the adsorption processes will be a major step forward to a realistic application of biomass-based nanocomposite for phosphate removal in the future.

2. MATERIALS AND METHODS

2.1. Materials. All chemicals involved in this study were of reagent grade, and solutions were all prepared by deionized water (18.2 MΩ cm). Zirconium oxychloride ($ZrOCl_2{\cdot}8H2O$) was purchased from Sigma-Aldrich Co. Aqueous stock containing 1000 mg P-PO_4^{3-}/L of orthophosphate was prepared by dissolving NaH_2PO_4 into deionized water. Wheat straw, a typical agricularal byproduct, was obtained from Lian Yungang, Jiangsu, China. It was divided into irregular-shaped particles ranging from 0.8 to 1.2 mm in diameter. Prior to use, wheat straw particle (Ws) was subjected to flushing with NaOH solution (0.1 M) followed by rinsing with deionized water until neutral pH, then washed by ethanol to remove the residual impurities, and dried under vacuum at 323 K for 12 h for further use. Other chemicals were provided by Shanghai Reagent station (Shanghai, China).

2.2. Preparation of the Biomass-Based Adsorbents. *Synthesis of Biomass-Based Anion Exchanger Ws−N.* To synthesize the biomass-based anion-exchanger Ws−N, 5 g of dried Ws was first swollen by 100 mL of *N*,*N*-dimethylformamide (DMF) at ambient temperature for 1 h, and then 25 mL of epichlorohydrin was added to

DOI: 10.1021/acsami.5b06098
ACS Appl. Mater. Interfaces 2015, 7, 20835−20844

the mixture as etherification agent and stirred for 2 h at 358 K. Quarternary amination groups were then introduced by adding 25 mL of triethylamine through titration, and the mixture was stirred for 3 h at 358 K. The reaction product was washed with 1 L of NaOH (0.1 M), 1 L of HCl (0.1 M), and 1 L of 50% ethanol solution. The product Ws−N was converted into Cl-type by washing with a certain amount of NaCl (0.5 M) at ambient temperature. The related synthetic procedure is illustrated in Figure 1.

Fabrication of the Nanocomposite Ws−N−Zr. In detail, 5 g of dried St-N was added into 100 mL of $ZrOCl_2{\cdot}8H_2O$ solution (0.5 M). The mixture was stirred for 6 h to allow the uptake of Zr(IV) onto the inner surface of Ws−N through a typical anion-exchange process. The Zr(IV) loaded Ws−N particles were then filtered, vacuum-desiccated, and immersed into 100 mL of 0.1 M NaOH−NaCl solution with continuous stirring at 298 K for 6 h. The preloaded Zr(IV) was in situ precipitated as hydrous zirconium oxide onto the inner surface of Ws−N. The resulting particles were flushed with DI water until neutral pH, and heated at 323 K for 24 h to obtain the nanocomposite Ws−N−Zr. Prior to use, the OH-type Ws−N−Zr was transformed to Cl-type by immersing the particles into 0.5 M NaCl solution, and then rinsed with DI water to approach circumneutral pH's. Fabrication of the nanocomposite Ws−N−Zr was schematically illustrated in Figure 2.

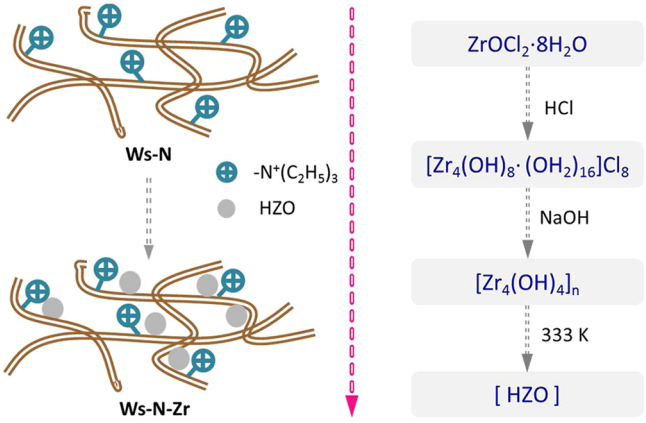

Figure 2. Schematic illustration for preparation procedure of Ws−N−Zr.

2.3. Phosphate Adsorption Experiments. Batch adsorption experiments were conducted by using a traditional bottle-point method. Fifty milligrams of dry adsorbent particles (Ws−N or Ws−N−Zr) was equilibrated in 250 mL flasks with 100 mL of solution at different initial phosphate levels. In isothermal study, the range of initial concentration of phosphate was set from 0.08 to 1.93 mmol P/L. The flasks were transferred to a thermostatic shaker and then shaken at 150 rpm for 24 h at 298 K. To study the effect of pH and coexisting anions on phosphate uptake, the initial concentration of phohphate was set as 0.32 mmol/L. An appropriate amount of HCl (0.10 M) or NaOH (0.10 M) solutions was used to adjust the solution pH, and Na_2SO_4 solution was added as the source of the competing anions when necessary. Preliminary kinetic experiments indicated that 10 h was sufficient to reach adsorption equilibrium onto Ws−N or Ws−N−Zr. Adsorption kinetics was performed by introducing 50 mg of adsorbent to 1000 mL of solution containing 0.32 mmol P/L of phosphate, and a 0.5 mL aliquot of supernatant was sampled at various time intervals for data analysis. The uptake amount was obtained on the basis of a mass balance between the initial and final phosphate concentrations.

2.4. Characterization and Analyses. The nanoparticles of hydrous zirconium oxide loaded on Ws−N were observed with transmission election microscopy (JEOL, JEM-2100 HR, Japan). The mineralogy of loaded HZO was determined by powder X-ray diffraction analysis instrument (XRD, XTRA, Switzerland) with Cu Kα radiation (40 kV, 25 mA). The effect of solution pH on Zr/biomass leaching from Ws−N−Zr was measured to evaluate the stability in water. The result of biomass leaching was examined by TOC analyzer (Shimadzu TOC-$L_{CPH/CPN}$). An inductive coupled plasma (ICP) emission spectrometer (PerkinElmer model Optima 5300DV) was used to determine Zr(IV) concentration in solution, and the Zr(IV) amount loaded within Ws−N was measured after the sample was digested into a HNO_3−$HClO_4$ solution. The phosphate concentration of solution samples, after being filtered through 0.45 mm syringe filter, was detected using a UV−vis spectrophotometer with molybdenum blue method.[29] The specific surface area and the pore size distribution of the adsorbents were measured by N_2 adsorption at 77 K on a Micromeritics ASAP-2010C Instrument (U.S.). Total nitrogen content of the samples was determined using a Perker-Elmer Elemental analyzer CHNS/O (model 2400II).

3. RESULTS AND DISCUSSION

3.1. Characterization of the Materials. The resulting adsorbent Ws−N, Ws−N−Zr was present as platy-shaped, thin particles of light-yellow color, same as the raw Ws. From the result of scanning electron micrographs, some distinct curved gullies and eyelets were seen on the external surface of raw Ws (Figure S1). After HZO was immobilized, the number of gullies was increased apparently as shown in Figure 3a, indicating the possibility to possess larger specific surface area for Ws−N−Zr. The diameter of eyelets on the external surface of Ws−N−Zr having a slight decrease might be caused by the pore clogging in HZO encapsulation. The TEM image of hybrid Ws−N−Zr depicted in Figure 3b indicates that HZO nanoparticles with

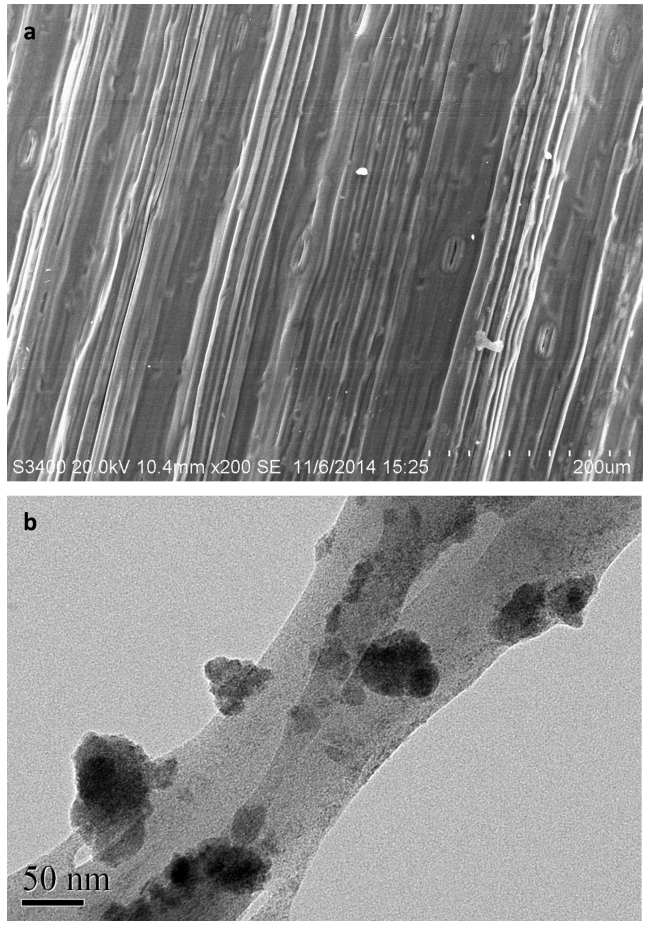

Figure 3. Characterization of the resultant Ws−N−Zr: (a) SEM image; (b) TEM image.

DOI: 10.1021/acsami.5b06098
ACS Appl. Mater. Interfaces 2015, 7, 20835−20844

sizes of about 50 nm were uniformly loaded onto the inner surface of the carrier.

The basic properties of three samples were summarized in Table 1. As compared to Ws and Ws−N, an increase in BET

Table 1. Physicochemical Properties of the Ws, Ws−N, and Ws−N−Zr

properties	samples		
	Ws	Ws−N	Ws−N−Zr
matrix structure	cellulose, hemicellulose, lignin		
BET surface area (m^2/g)	5.58	5.62	54.61
average pore diameter (nm)	4.06	4.08	3.25
pore volume (cm^3/g)	6.99×10^{-3}	6.49×10^{-3}	8.75×10^{-2}
surface functional groups	R−OH	R−OH/R−$N^+(CH_2CH_3)_3$	R−OH/R−$N^+(CH_2CH_3)_3$/HZO
HZO content (Zr mass %)			19.3%

data of Ws−N−Zr was obtained due to the presence of nanosized HZO, which generally have greater accessible surface area and more active adsorption sites.[19,30] In addition, both the average pore diameter and the pore volume of Ws−N−Zr fell due to the pore blockage as a result of HZO encapsulation. It can be concluded that the loaded HZO nanoparticle provides a higher surface area, although they might block some of the inner pores of the biomass carrier. According to the wide-angle XRD patterns of Ws, Ws−N, and Ws−N−Zr, most HZO nanoparticles impregnated inside Ws−N are amorphous in nature (Figure S2). ICP-MS measurement showed that the Zr(IV) loading amount of Ws−N−Zr was 19.3% in Zr mass after acidic digestion, resulting in a higher apparent density than Ws.

The results of elemental analysis for the natural and synthetic samples are given in Table S1. The systhetic Ws−N and Ws−N−Zr had nitrogen contents of 1.49% and 0.89%, respectively, suggesting that quaternary ammonium groups have successfully grafted on the matrix of raw wheat straw. The calculated total exchange capacity (TEC) was based on the nitrogen content incorporated into the final products based on the equation TEC ($mEq \cdot g^{-1}$) = N%/1.4. The TEC value of Ws−N−Zr was 0.64 $mEq \cdot g^{-1}$, lower than that of Ws−N (1.06 $mEq \cdot g^{-1}$), which is mainly due to the higher density after HZO nanoparticle was loaded.

The effect of solution pH on the stability of Ws−N−Zr was examined, as shown in Figure 4. Less than 1 $\mu g/L$ Zr(IV) (<0.05%) was leaching into the surrounding solution over the whole pH range after being immersed for 48 h. The Ws−N−Zr exhibited much better acidic resistance, as compared to other metal oxide-contained nanocomposite adsorbents. For instance, nearly 80% iron oxides encapsulated inside polymeric resin were dissolved and leached into solution at pH = 2.0 for 24 h.[31] Such performance is very attractive because phosphate ions are widespread in different types of waters, that is, acidic mining effluents, electroplating wastewater, etc. The TOC result was also detected to test the stability of Ws−N−Zr in case the organic matter of the biomass carrier releasing to the solution. The maximum value of TOC was nearly 4 mg/L, present at pH = 2. Basically, the TOC concentration was below 2 mg/L when the pH was 4−10 after 48 h of immersion, which enables wheat

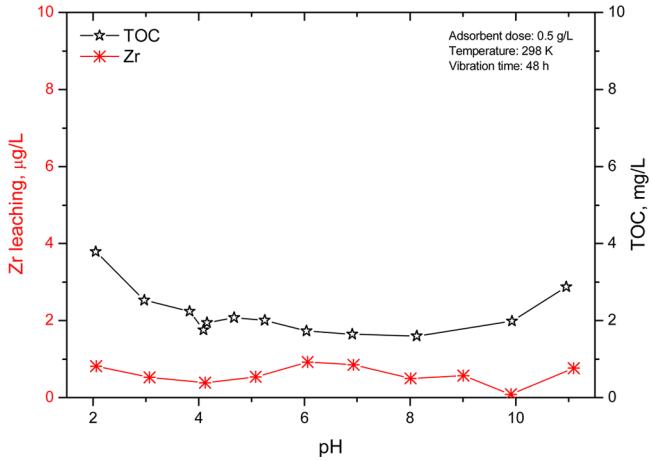

Figure 4. pH-Dependent Zr(IV)/TOC leaching from Ws−N−Zr particles for 48 h shaking at 303 K.

straw to be an appropriate support within a broader pH range. The results implied that the nanocomposite Ws−N−Zr could be a promising adsorbent for phosphate removal with a significant advantage of excellent chemical stablility.

3.2. Comparative Study on the Absorption Capability of Three Samples. As is well-known, adsorption capacity is an important parameter in evaluating the performance of adsorbents. Here, we conducted the adsorption isotherm experiments of phosphate onto the three samples at 298 K. The results shown in Figure 5 illustrated that the adsorption

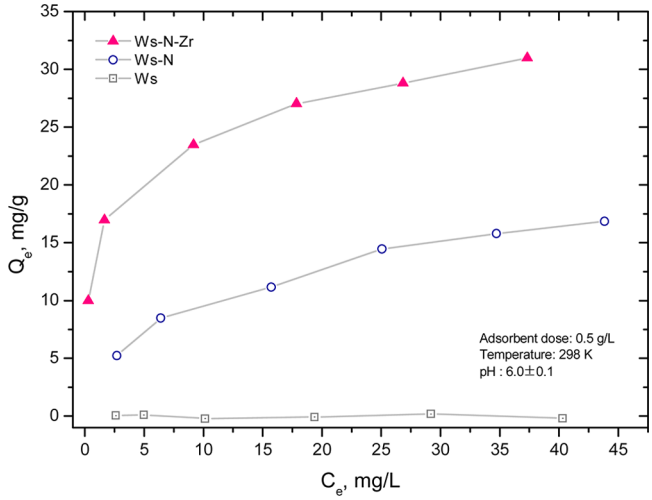

Figure 5. Phosphate adsorption isotherms of Ws, Ws−N, and Ws−N−Zr at 298 K.

capacity of Ws was nearly zero; that is to say, the hydroxyl groups carried by raw wheat straw cannot be used as active adsorption sites for phosphate. After being modified by quaternary ammonia groups, the resultant biomass-based anion exchanger Ws−N exhibits obvious adsorption capability for phosphate, which can be attributed to Coulombic interaction between quaternary ammonia groups and phosphate ions. After being fit by the Langmuir isotherm model, the maximum adsorption capacity was obtained as about 19.5 mg/g. As for hybrid Ws−N−Zr, the maximum adsorption amount was calculated as about 31.9 mg/g, displaying higher adsorption capacity than other samples. The superior performance of Ws−

DOI: 10.1021/acsami.5b06098
ACS Appl. Mater. Interfaces 2015, 7, 20835−20844

N−Zr can be elucidated on the basis of its specific two-site structure, the Donnan membrane effect exerted by the immobilized quaternary ammonia groups bound to the biomass matrix, as well as the impregnated HZO nanoparticles of specific interaction toward phosphate.[32]

3.3. FTIR and XPS Study. The novel biomass-based zirconium oxide nanocomposite with excellent performance toward phosphate was successfully prepared, and the adsorption mechanism was further explored by microscopic technique of FTIR and XPS. Figure 6 illustrated the FTIR spectra of Ws−N−Zr before and after phosphate adsorption, respectively. Before adsorption, the FTIR spectrum of Ws−N−Zr had a strong and broad band at 3381 cm^{-1} (O−H stretching vibration) and a band at 1638 cm^{-1} (O−H bending vibration), indicating the presence of coordinated water molecules, as well as the peak at 1338 cm^{-1} (O−H bending vibration), indicating the presence of surface hydroxyl on the nanocomposite (mostly Zr−OH).[18] After adsorption, the O−H bending vibration peak of surface hydroxyl (1338 cm^{-1}) disappeared, while the peak of coordinated water molecules (1638 cm^{-1}) weakened. The decreasing tendency of these two peaks indicated that the surface hydroxyl groups might be replaced by adsorbed phosphate. The FTIR results confirmed that the substitution of −OH groups by phosphate species played a key role in their adsorption on Ws−N−Zr, revealing the formation of inner-sphere complexation between phosphate and the loaded HZO.

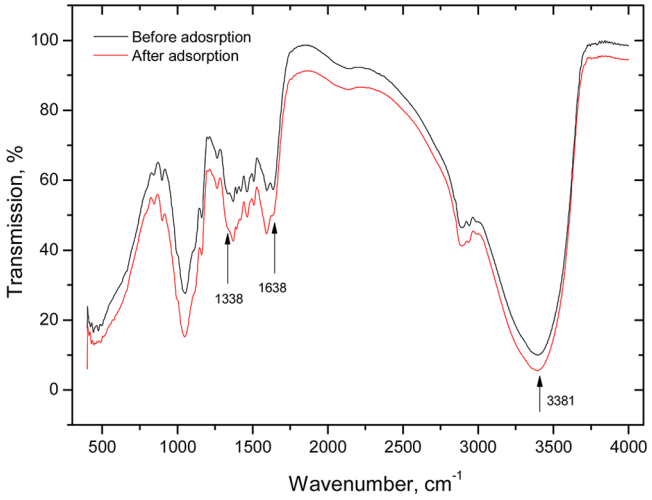

Figure 6. FTIR spectra of Ws−N−Zr before and after phosphate adsorption (initial P, 10 mg/L; adsorption dose, 0.5 g/L; pH, 6.0 ± 0.1; *T*, 298 K).

The XPS survey scan of Ws−N−Zr before and after phosphate adsorption was shown in Figure 7a. As compared to the primitive Ws−N−Zr, the new P 2p peak can be observed on the spectra of phosphate-loaded Ws−N−Zr, which can indicate that phosphate was successfully adsorbed on the nanocomposite. Figure 7b displayed the binding energy of the P 2p peak for NaH_2PO_4 centered at 133.8 eV. However, a remarkable shift to lower binding energy of 132.4 eV was observed for the phosphate-loaded Ws−N−Zr, suggesting the formation of strong chemical bonding between phosphate and Ws−N−Zr. The peaks of Zr $3d_{5/2}$ and Zr $3d_{3/2}$ for primitive Ws−Zr−N are centered at about 181.2 and 183.6 eV, respectively (Figure 7c). After phosphate adsorbed, a slight peak shift to higher binding energy was observed for Zr 3d spectra (Figure 7d), indicating a noticeable change in Zr species. A deconvolution in which the Zr $3d_{5/2}$ and $3d_{3/2}$ spectra are assumed to be composed of two overlapping peaks was undertaken. The new peaks were located at 181.7 and 184.1 eV, respectively, which can be attributed to the new Zr species that originated from the formation of inner-sphere complexation with phosphate.

Figure 7e and f illustrated the O 1s spectra of Ws−N−Zr before and after phosphate adsorption. The O 1s peak could be best fitted with three overlapped O 1s peaks of oxide oxygen (O^{2-}), hydroxyl group (−OH), and carbon oxygen (C−O), which originated from the biomass carrier. The −OH percentage was about 34.4% for primitive Ws−N−Zr, while it dropped to about 21.2% after phosphate adsorption. It can be concluded that hydroxyl groups existed on the surface of HZO nanoparticles, and the −OH percentage in the total surface oxygen dropped apparently after phosphate adsorption. Therefore, the decrease of −OH groups could be attributed to the replacement of −OH by phosphate during the adsorption process, which is in accordance with the results of the FTIR study.

3.4. Effect of Solution pH. Figure 8 described the effect of solution pH on phosphate removal by Ws−N−Zr and Ws−N. The optimum pH values for phosphate adsorption by Ws−N range from 6 to 8. For hybrid Ws−N−Zr, the adsorption capacity shows an apparent rise as the pH is declining. It is known that phosphate is polyacidic with three pK_a values (2.12, 7.21, and 12.31).[33] The decreasing pH values inevitably result in phosphate (usually $H_2PO_4^-$ or HPO_4^{2-}) being less negatively charged, that is, formation of more H_3PO_4 or $H_2PO_4^-$, which was unfavorable for its retention by ammonium groups of Ws−N through the Coulombic interaction. At higher pH, although the fraction of multicharged phosphate anions (e.g., HPO_4^{2-} or PO_4^{3-}) increased, the increasing concentration of hydroxyl ions would compete for the adsorption sites with phosphate, leading to the declined adsorption amount for phosphate by Ws−N.

For hybrid Ws−N−Zr, two distinct sites can be used for phosphate adsorption, quaternary ammonium groups of host Ws−N and hydroxyl groups of loaded HZO nanoparticles. Both sites interact with phosphate ions by following eqs 1 and 2:[23]

$$\overline{a\text{R}-\text{N}^+(\text{CH}_2\text{CH}_3)_3\text{Cl}^-} + \text{H}_x\text{PO}_4^{(3-x)-}(\text{aq}) \rightarrow \overline{[\text{R}-\text{N}^+(\text{CH}_2\text{CH}_3)_3]_a[\text{H}_x\text{PO}_4^{(3-x)-}]} + a\text{Cl}^-(\text{aq}) \quad (1)$$

$$\overline{\text{Zr}-(\text{OH})_y} + b\text{H}_x\text{PO}_4^{(3-x)-}(\text{aq}) \rightarrow \overline{\text{Zr}-(\text{OH})_{y-b}[\text{H}_x\text{PO}_4^{(3-x)-}]_b} + b\text{OH}^-(\text{aq}) \quad (2)$$

At higher pH, in addition to the competition effect of −OH, HZO is deprotonated and became negatively charged. Hence, electrostatic repulsive forces between HZO and phosphate ions made a dominant contribution, which is favorable for desorption of adsorbed phosphate ions.[34] At a lower pH value, the increasing solution acidity would drive eq 2 forward and facilitate the adsorption by HZO particles, counteracting the opposite effect caused by quaternary ammonium groups. Therefore, the phosphate adsorption by hybrid Ws−N−Zr still was maintained at a relatively high level at low pH region. From Figure 8, we can conclude that the new synthetic nanocomposite Ws−N−Zr can be employed in neutral or acidic

DOI: 10.1021/acsami.5b06098
ACS Appl. Mater. Interfaces 2015, 7, 20835−20844

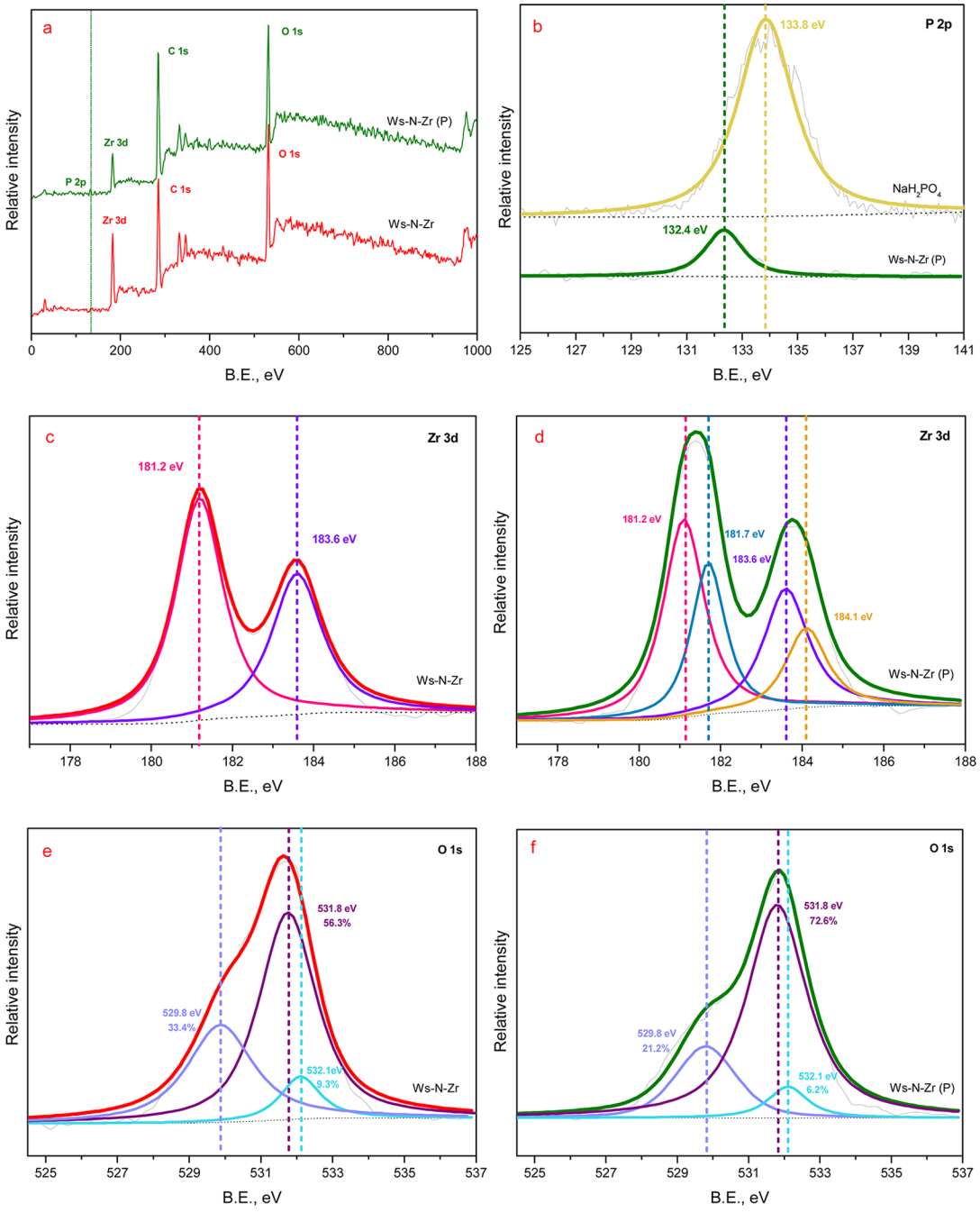

Figure 7. XPS analysis of the nanocomposite Ws−N−Zr before or after phosphate adsorption. (a) XPS survey scan of Ws−N−Zr before or after phosphate adsorption; (b) P 2p spectra of NaH_2PO_4 and phosphate loaded Ws−N−Zr; (c,d) Zr $3d_{5/2}$ and $3d_{3/2}$ spectra before and after phosphate adsorption; and (e,f) O 1s spectra before and after phosphate adsorption.

waters, also meeting the actual situation for wastewaters in advanced treatment. Moreover, thanks to the pH effect, the exhausted nanocomposite Ws−N−Zr can be regenerated with proper alkaline solution to achieve the purpose of cyclic utilization. The details are discussed later.

3.5. Effect of Sulfate Ions. It is of great importance to evaluate the selectivity of the nanocomposite toward phosphate because coexisting anions are commonly present in natural waters or wastewaters, such as Cl^-, NO_3^-, and SO_4^{2-}.[35] They are supposed to compete with phosphate for active sites of given adsorbent. Here, SO_4^{2-} was selected as a representative background ion considering it shows a stronger competitive impact on target pollutant than others.[36] The synthetic biomass anion exchanger Ws−N and commercial anion exchanger IRA-900 were employed for reference. The experimental data were depicted in Figure 9. When the molar ratio of sulfate:phosphate increased from 0 to 60, Ws−N−Zr still performed 70−80% removal efficiency for phosphate, while that of IRA-900 or Ws-N declined to nearly zero. The hybrid Ws−N−Zr exhibited much higher capacity than IRA-900 and Ws−N in a competitive background. The reason lies in that the reference IRA-900 or Ws−N sequesters phosphate only through a nonspecific ion exchange or Coulombic interaction, and the presence of coexist anions would occupy the active sites for competition. Yet for hybrid Ws−N−Zr, in addition to the nonspecific interaction between quaternary ammonium groups

DOI: 10.1021/acsami.5b06098
ACS Appl. Mater. Interfaces 2015, 7, 20835−20844

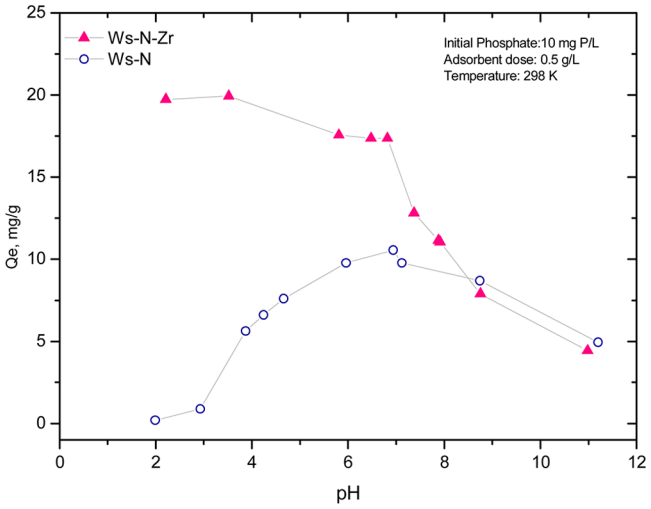

Figure 8. Effect of solution pH on the phosphate retention by synthetic Ws−N and Ws−N−Zr.

and phosphate, the impregnated HZO nanoparticles could exhibit preferable adsorption toward phosphate through formation of the inner-sphere complexes, which can be explained by the principle of hard and soft acids and bases (the HSAB principle).[18,37] HZO nanoparticles are supposed to act as a soft Lewis acid and the phosphate ions act as a soft Lewis base to denote electron pairs to bind Zr atom, and then the inner-sphere complexes are formed.[23] The coexisting anions have difficulty competing for active adsorption sites on encapsulated HZO nanoparticles. Thus, after the initial falling of adsorption, a further increase in coexist anions did not affect phosphate removal by Ws−N−Zr significantly.

Phosphate adsorption isotherm of Ws−N−Zr in the presence of 500 mg/L sulfate ions was also performed to evaluate the adsorption capability in strongly competitive background (Figure 8). The maximum adsorption capacity was calculated to be 24.8 mg/g for Ws−N−Zr, which exhibits a much higher performance over the polymer-based hydrated ferric oxide reported in the previous research.[38] In summary, as compared to other reported adsorbents, this new biomass-based HZO nanoparticle displays apparently preferable adsorption ability for phosphate ions.

3.6. Adsorption Kinetics. Adsorption kinetics of phosphate on Ws−N−Zr and Ws−N were examined, and the results are presented in Figure 10. An initial fast adsorption was observed for both materials, followed by a slow state, and the adsorption equilibrium was achieved within 120 min for Ws−N−Zr and 100 min for Ws−N, respectively. Theoretically, adsorption rate depends on the mass transport rate of phosphate ions within the inner pore of synthetic Ws−N−Zr. Here, a widely used kinetic model, intraparticle diffusion model, was employed to fit the kinetic data.[39] The equation was described as follows:

$$Q_t = k_i t^{0.5} + C$$

where Q_t is the phosphate amount adsorbed at time t (mg/g), k_i is the diffusion rate constant (mg/g·min$^{0.5}$), and C is the intercept for any experiment.

The plot of Q_t versus $t^{0.5}$ may present a multilinearity, which reveals that two or more steps occur in the adsorption. The k_{i1} and k_{i2} represent diffusion rates of the different stages in adsorption process.[40] The results in Figure 10 indicated that the intraparticle diffusion model described the data well, and the determination coefficients R^2 for step 1 and step 2 were 0.995 and 0.982, respectively (Table S2). The initial part is the external surface adsorption controlled by film diffusion. Phosphate ions were adsorbed by the exterior surface of the Ws−N−Zr particle, so the adsorption rate was fast in the beginning. The second part is the gradual adsorption stage, where intraparticle diffusion is the rate-controlling step. When adsorption by the exterior surface of the particle reached saturation, phosphate ions entered into the inner pore region and adsorbed by the interior surface of Ws−N−Zr. The diffusion resistance increased when phosphate ions diffused inside the pore of the particle, causing the diffusion rate to decline. The third portion is the final equilibrium stage, where the rates of adsorption and desorption remain equivalent. Therefore, the changes of k_{i1}(2.161), k_{i2}(0.877) could be attributed to the different adsorption stages controlled by film and intraparticle diffusion.

3.7. Cycle Experiments. Cycle adsorption and regeneration of batch experiments were taken to evaluate the reusability of Ws−N−Zr for phosphate removal. The adsorbent dosage for the first cycle was set as 1 g/L, and the initial P concentration was set at 20 mg/L. The regeneration of the

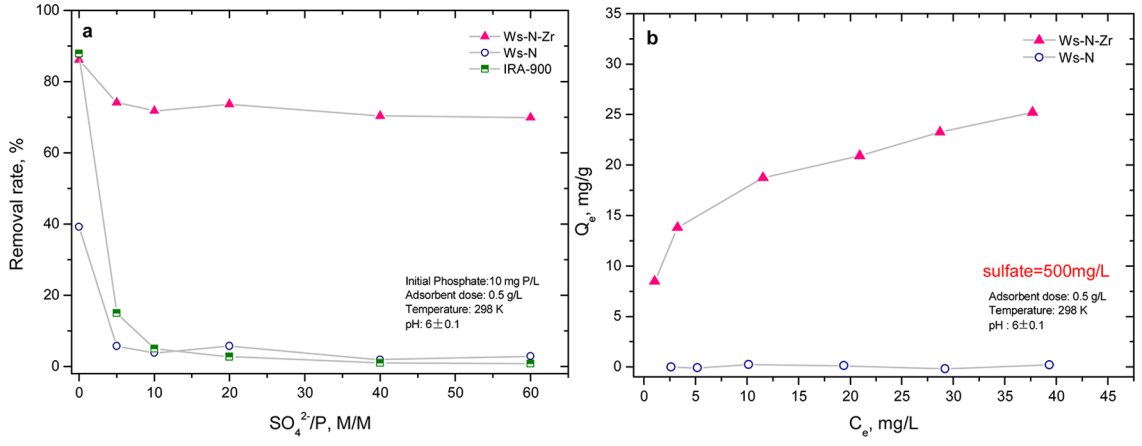

Figure 9. Phosphate uptake onto different adsorbents in sulfate background at 298 K. (a) Effect of various sulfate concentration on phosphate removal; and (b) phosphate adsorption isotherms in the presence of 500 mg/L sulfate ions.

DOI: 10.1021/acsami.5b06098
ACS Appl. Mater. Interfaces 2015, 7, 20835−20844

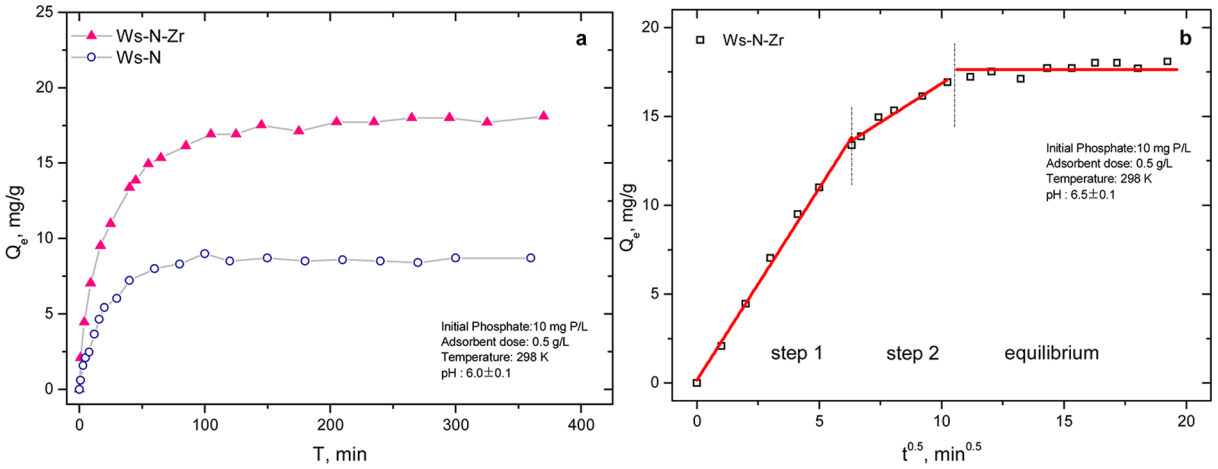

Figure 10. (a) Adsorption kinetics of phosphate for Ws−N and Ws−N−Zr at 298 K; and (b) intraparticle diffusion modeling results of phosphate adsorption by Ws−N−Zr.

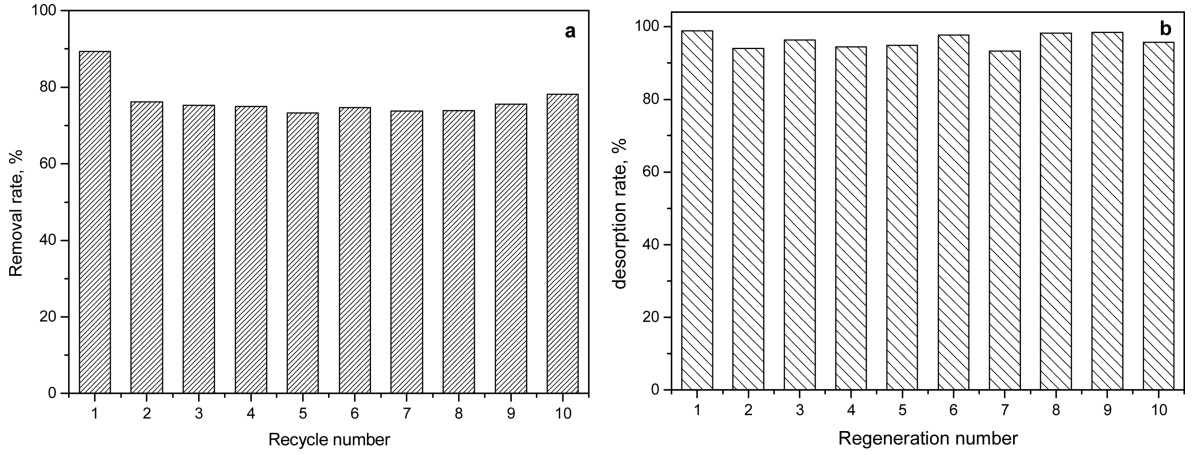

Figure 11. Cycle adsorption and regeneration of batch experiments for nanocomposite Ws−N−Zr. (a) Adsorption cycle; (b) regeneration cycle (initial P, 20 mg/L; adsorption dose, 1 g/L; pH, 6.0 ± 0.1; *T*, 298 K).

exhausted Ws−N−Zr was performed by using the binary NaOH−NaCl (5 wt %) solution at ambient temperature. Before the next cycle adsorption, the nanocomposite was rinsed with 0.1 M NaCl solution to transfer Ws−N−Zr from OH type to Cl type.

The cycle adsorption results are illustrated in Figure 11a; phosphate removal efficiency of Ws−N−Zr was about 89.4% for the first cycle, and the desorption efficiency was up to 98.2% (Figure 11b). In the second cycle, the removal efficiency has dropped to 76.5%, implying a slight fraction of active sites are irreversible after regeneration.[41] Despite that, subsequent cycle 2−10 adsorption tests proved that the removal rate of phosphate was maintained above 70% without further capacity loss. The preloaded phosphate could be effectively desorbed with regeneration efficiency >94% for all of the 10-cycle tests. In the first regeneration, some HZO nanoparticles attached on the surface of hybrid Ws−N−Zr might be washed off, leading to the decrease in phosphate uptake in the second adsorption cycle. The loaded HZO in the inner surface of composite would not be much affected, so the phosphate uptake in the subsequent cycles tended to level off. On the basis of that, we can reasonably predict that the adsorption capacity would remain stable even after the tenth cycle.

Note that the morphology of metal oxides would be easy to change under alkaline conditions, which might result in declining adsorption ability.[42] Considering that, we examined the morphology of HZO nanoparticle of Ws−N−Zr after the tenth regeneration through XRD patterns. The result (Figure 12) is highly consistent with the raw Ws−N−Zr, showing

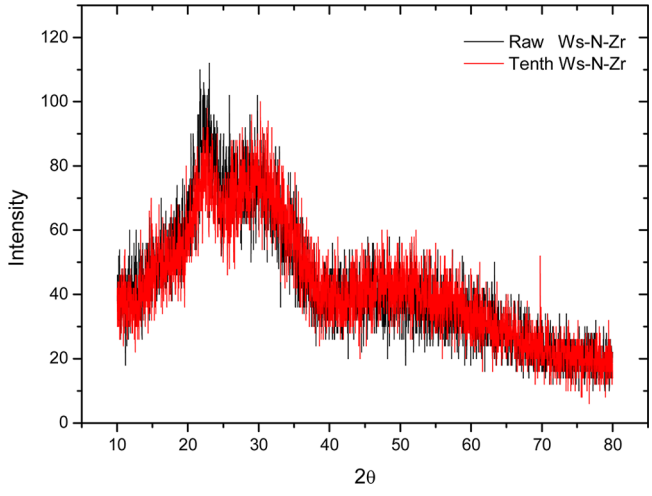

Figure 12. XRD spectra of Ws−N−Zr for raw material and after 10 cycles' regeneration.

DOI: 10.1021/acsami.5b06098
ACS Appl. Mater. Interfaces 2015, 7, 20835−20844

excellent stability in impregnated HZO nanoparticle. Besides, the TEM image (Figure S3) also indicated that the size of the HZO nanoparticle after 10 cycles' regeneration was still about 50 nm, same as the primitive one. On the basis of the results of XRD pattern and TEM image, no significant structure change was observed on the surface morphology of Ws−N−Zr in the regeneration process. We also measured Zr(IV) content in solution after each cycle test; no zirconium species were detected in solution at ambient pH, implying its feasible application in water treatment. Consequently, it can be concluded that the nanocomposite Ws−N−Zr could be employed for preferable phosphate removal without any significant capacity loss in recycle use.

4. CONCLUSIONS

A low-cost, eco-friendly nanocomposite with high removal activity toward phosphate was newly developed by immobilizing hydrated zirconium oxide on the inner surface of wheat straw, which has been modified by quaternary ammonium salts. As compared to widely used commercial anion exchangers, modified biomass material was selected as the carrier mainly because it can avoid high costs and secondary pollution in the preparation. The novel adsorbent Ws−N−Zr could effectively capture phosphate ions in pH 2−7 without any Zr(IV) leaching through two distinct processes: nonspecific ion exchange by quaternary ammonium groups of wheat straw and specific inner-sphere complexation by impregnated HZO nanoparticles. The FTIR and XPS study confirmed that the substitution of −OH groups by phosphate species played a key role in their adsorption on Ws−N−Zr, revealing the formation of inner-sphere complexation between phosphate and the loaded HZO.

Therefore, Ws−N−Zr displays selective adsorption ability to phosphate than other common anions such as sulfate. Cycle adsorption and regeneration of batch experiments demonstrated that Ws−N−Zr could be employed for repeated use without significantly capacity loss, when the binary NaOH−NaCl solution was employed as the regenerative agent. Considering the facile separation of Ws−N−Zr due to its large particle size, HZO nanoparticle immobilization within quaternary-aminated wheat straw can be considered as an effective and low-priced approach to greatly improve the applicability of Zr(IV) oxides for large-scale environmental remediation.

■ ASSOCIATED CONTENT

Supporting Information

The Supporting Information is available free of charge on the ACS Publications website at DOI: 10.1021/acsami.5b06098.

SEM image of the raw wheat straw (Ws); XRD spectra of the three samples; elemental analysis and TEC values of Ws, Ws−N, Ws−N−Zr; intraparticle diffusion model parameters of phosphate adsorption onto Ws−N−Zr; and TEM image of Ws−N−Zr after 10 cycles' regeneration (PDF)

■ AUTHOR INFORMATION

Corresponding Authors

*Tel.: +86-25-5873-1090. Fax: +86-25-5873-1090. E-mail: hqiu@nuist.edu.cn.

*E-mail: zxlwinner@126.com.

Notes

The authors declare no competing financial interest.

■ ACKNOWLEDGMENTS

The study was financially supported by the NSFC (41401546, 21272118, 21501097). Meanwhile, this work was supported by A Project Funded by the Priority Academic Program Development of Jiangsu Higher Education Institutions (PAPD), Jiangsu Joint Laboratory of Atmospheric Pollution Control, and Jiangsu Engineering Technology Research Center of Environmental Cleaning Materials.

■ REFERENCES

(1) Conley, D. J.; Paerl, H. W.; Howarth, R. W.; Boesch, D. F.; Seitzinge, S. P.; Havens, K. E.; Lancelot, C.; Likens, G. E. Controlling Eutrophication: Nitrogen and Phosphorus. *Science* **2009**, *323*, 1014−1015.

(2) Loganathan, P.; Vigneswaran, S.; Kandasamy, J.; Bolan, N. S. Removal and Recovery of Phosphate from Water Using Sorption. *Crit. Rev. Environ. Sci. Technol.* **2014**, *44*, 847−907.

(3) Sharpley, A. N.; Daniel, T.; Sims, T.; Lemunyon, J.; Stevens, R.; Parry, R. Agricultural Phosphorus and Eutrophication. *United States Department of Agriculture, Agricultural Research Service*, 2nd ed.; United States Department of Agriculture, Agricultural Research Service, 2003.

(4) Seviour, R. J.; Mino, T.; Onuki, M. The Microbiology of Biological Phosphorus Removal in Activated Sludge Systems. *FEMS Microbiology Reviews* **2003**, *27*, 99−127.

(5) Tang, Y. Q.; Zong, E. M.; Wan, H. Q.; Xu, Z. Y.; Zheng, S. R.; Zhu, D. Q. Zirconia Functionalized SBA-15 as Effective Adsorbent for Phosphate Removal. *Microporous Mesoporous Mater.* **2012**, *155*, 192−200.

(6) Qiu, G. L.; Law, Y. M.; Das, S.; Ting, Y. P. Direct and Complete Phosphorus Recovery from Municipal Wastewater Using a Hybrid Microfiltration-Forward Osmosis Membrane Bioreactor Process with Seawater Brine as Draw Solution. *Environ. Sci. Technol.* **2015**, *49*, 6156−6163.

(7) Gifforda, M.; Liu, J. Y.; Rittmann, B. E.; Vannela, R.; Westerhoff, P. Phosphorus Recovery from Microbial Biofuel Residual Using Microwave Peroxide Digestion and Anion Exchange. *Water Res.* **2015**, *70*, 130−137.

(8) Vale, P. Chemical Dosing: Challenges and Opportunities. *Conference on Low Energy Wastewater Treatment Systems*; Cranfield University: England, 2013.

(9) Oehmen, A.; Lemos, P. C.; Carvalho, G.; Yuan, Z. G.; Keller, J.; Blackall, L. L.; Reis, M. A. M. Advances in Enhanced Biological Phosphorus Removal: from Micro Tomacro Scale. *Water Res.* **2007**, *41*, 2271−2300.

(10) Desmidt, E.; Ghyselbrecht, K.; Zhang, Y.; Pinoy, L.; Bruggen, B. V. D.; Verstraete, W.; Rabaey, K.; Meesschaert, B. Global Phosphorus Scarcity and Full-Scale P-Recovery Techniques: A Review. *Crit. Rev. Environ. Sci. Technol.* **2015**, *45*, 336−384.

(11) Pan, B. C.; Han, F. C.; Nie, G. Z.; Wu, B.; He, K.; Lv, L. New Strategy To Enhance Phosphate Removal from Water by Hydrous Manganese Oxide. *Environ. Sci. Technol.* **2014**, *48*, 5101−5107.

(12) Huang, W. Y.; Zhu, Y.; Tang, J. P.; Yu, X.; Wang, X. L.; Li, D.; Zhang, Y. M. Lanthanum-Doped Ordered Mesoporous Hollow Silica Spheres as Novel Adsorbents for Efficient Phosphate Removal. *J. Mater. Chem. A* **2014**, *2*, 8839−8848.

(13) Khare, N.; Martin, J. D.; Hesterberg, D. Phosphate Bonding Configuration on Ferrihydrite Based on Molecular Orbital Calculations and XANES Fingerprinting. *Geochim. Cosmochim. Acta* **2007**, *71*, 4405−4415.

(14) Abdala, D. B.; Northrup, P. A.; Arai, Y.; Sparks, D. L. Surface Loading Effects on Orthophosphate Surface Complexation at the Goethite/Qater Interface as Examined by Extended X-ray Absorption Fine Structure (EXAFS) Spectroscopy. *J. Colloid Interface Sci.* **2015**, *437*, 297−303.

(15) Bhandari, N.; Hausner, D. B.; Kubicki, J. D.; Strongin, D. R. Photodissolution of Ferrihydrite in the Presence of Oxalic Acid: an in Situ ATR-FTIR/DFT Study. *Langmuir* **2010**, *26*, 16246−16253.

DOI: 10.1021/acsami.5b06098
ACS Appl. Mater. Interfaces 2015, 7, 20835−20844

(16) Qiu, H.; Zhang, S. J.; Pan, B. C.; Zhang, W. M.; Lv, L. Oxalate-Promoted Dissolution of Hydrous Ferric Oxide Immobilized Within Nanoporous Polymers: Effect of Ionic Strength and Visible Light Irradiation. *Chem. Eng. J.* **2013**, *232*, 167−173.
(17) Rodrigues, L. A.; Maschio, L. J.; Coppio, L. D. S. C.; Thim, G. P.; Silva, M. L. C. P. D. Adsorption of Phosphate from Aqueous Solution by Hydrous Zirconium Oxide. *Environ. Technol.* **2012**, *33*, 1345−1351.
(18) Su, Y.; Cui, H.; Li, Q.; Gao, S.; Shang, J. K. Strong Adsorption of Phosphate by Amorphous Zirconium Oxide Nanoparticles. *Water Res.* **2013**, *47*, 5018−5026.
(19) Hua, M.; Jiang, Y. N.; Wu, B.; Pan, B. C.; Zhao, X.; Zhang, Q. X. Fabrication of a New Hydrous Zr(IV) Oxide-Based Nanocomposite for Enhanced Pb(II) and Cd(II) Removal from Waters. *ACS Appl. Mater. Interfaces* **2013**, *5*, 12135−12142.
(20) Acelasa, N. Y.; Martinb, B. D.; Lópeza, D.; Jefferson, B. Selective Removal of Phosphate from Wastewater Using Hydrated Metal Oxides Dispersed Within Anionic Exchange Media. *Chemosphere* **2015**, *119*, 1353−1360.
(21) Yang, M. J.; Lin, J. W.; Zhan, Y. H.; Zhang, H. H. Adsorption of Phosphate from Water on Lake Sediments Amended With Zirconium-Modified Zeolites in Batch Mode. *Ecol. Eng.* **2014**, *71*, 223−233.
(22) Sandoval, R.; Cooper, A. M.; Aymar, K.; Jain, A.; Hristovski, K. Removal of Arsenic and Methylene Blue from Water by Granular Activated Carbon Media Impregnated with Zirconium Dioxide Nanoparticles. *J. Hazard. Mater.* **2011**, *193*, 296−303.
(23) Chen, L.; Zhao, X.; Pan, B. C.; Zhang, W. X.; Hua, M.; Lv, L.; Zhang, W. M. Preferable Removal of Phosphate from Water Using Hydrous Zirconium Oxide-Based Nanocomposite of High Stability. *J. Hazard. Mater.* **2015**, *284*, 35−42.
(24) Orlando, U. S.; Baes, A. U.; Nishijima, W.; Okada, M. Preparation of Agricultural Residue Anion Exchangers and Its Nitrate Maximum Adsorption Capacity. *Chemosphere* **2002**, *48*, 1041−1046.
(25) Orlando, U. S.; Baes, A. U.; Nishijima, W.; Okada, M. A New Procedure to Produce Lignocellulosic Anion Exchangers from Agricultural Waste Materials. *Bioresour. Technol.* **2002**, *83*, 195−198.
(26) Orlando, U. S.; Okuda, T.; Baes, A. U.; Nishijima, W.; Okada, M. Chemical Properties of Anion-Exchangers Prepared from Waste Natural Materials. *React. Funct. Polym.* **2003**, *55*, 311−318.
(27) Xu, X.; Gao, B. Y.; Wang, W. Y.; Yue, Q. Y.; Wang, Y.; Ni, S. Q. Effect of Modifying Agents on the Preparation and Properties of the New Adsorbents from Wheat Straw. *Bioresour. Technol.* **2010**, *101*, 1477−1481.
(28) Xu, X.; Gao, B. Y.; Yue, Q. Y.; Zhong, Q. Q. Preparation of Agricultural By-product Based Anion Exchanger and Its Utilization for Nitrate and Phosphate Removal. *Bioresour. Technol.* **2010**, *101*, 8558−8564.
(29) Tobey, S. L.; Jones, B. D.; Anslyn, E. V. C_{3v} Symmetric Receptors Show High Selectivity and High Affinity for Phosphate. *J. Am. Chem. Soc.* **2003**, *125*, 4026−4027.
(30) Aditya, D.; Rohan, P.; Suresh, G. Nano-Adsorbents for Wastewater Treatment: a Review. *Res. J. Chem. Environ.* **2011**, *15*, 1033−1040.
(31) Pan, B. J.; Qiu, H.; Pan, B. C.; Nie, G. Z.; Xiao, L. L.; Lv, L.; Zhang, W. M.; Zhang, Q. X.; Zheng, S. R. Highly Efficient Removal of Heavy Metals by Polymer-Supported Nanosized Hydrated Fe(III) Oxides: Behavior and XPS study. *Water Res.* **2010**, *44*, 815−824.
(32) Cumbal, L.; SenGupta, A. K. Arsenic Removal Using Polymer Supported Hydrated Iron(III) Oxide Nanoparticles: Role of Donnan Membrane Effect. *Environ. Sci. Technol.* **2005**, *39*, 6508−6515.
(33) Kubicki, J. D.; Paul, K. W.; Kabalan, L.; Zhu, Q.; Mrozik, M. K.; Aryanpour, M.; Pierre-Louis, A. M.; Strongin, D. R. ATR−FTIR and Density Functional Theory Study of the Structures, Energetics, and Vibrational Spectra of Phosphate Adsorbed onto Goethite. *Langmuir* **2012**, *28*, 14573−14587.
(34) Rodrigues, L. A.; Maschio, L. J.; Coppio, L. D. S. C.; Thim, G. P.; Silva, M. L. C. P. D. Adsorption of Phosphate from Aqueous Solution by Hydrous Zirconium Oxide. *Environ. Technol.* **2012**, *33*, 1345−1351.
(35) Pan, B. C.; Xu, J. S.; Wu, B.; Li, Z. G.; Liu, X. T. Enhanced Removal of Fluoride by Polystyrene Anion Exchanger Supported Hydrous Zirconium Oxide Nanoparticles. *Environ. Sci. Technol.* **2013**, *47*, 9347−9354.
(36) Qiu, H.; Zhang, S. J.; Pan, B. C.; Zhang, W. M.; Lv, L. Effect of Sulfate on Cu(II) Sorption to Polymer-Supported Nano-Iron Oxides: Behavior and XPS study. *J. Colloid Interface Sci.* **2012**, *366*, 37−43.
(37) Chitrakar, R.; Tezuka, S.; Sonoda, A.; Sakane, K.; Ooi, K.; Hirotsu, T. Selective Adsorption of Phosphate from Seawater and Wastewater by Amorphous Zirconium Hydroxide. *J. Colloid Interface Sci.* **2006**, *297*, 426−433.
(38) Pan, B. J.; Wu, J.; Pan, B. C.; Lv, L.; Zhang, W. M.; Xiao, L. L.; Wang, X. S.; Tao, X. C.; Zheng, S. R. Development of Polymer-Based Nanosized Hydrated Ferric Oxides (HFOs) for Enhanced Phosphate Removal from Waste Effluents. *Water Res.* **2009**, *43*, 4421−4429.
(39) Qiu, H.; Lv, L.; Pan, B. C.; Zhang, Q. J.; Zhang, W. M.; Zhang, Q. X. Critical Review in Adsorption Kinetic Models. *J. Zhejiang Univ., Sci., A* **2009**, *10*, 716−724.
(40) Wang, J.; Zhang, S. J.; Pan, B. C.; Zhang, W. M.; Lv, L. Hydrous Ferric Oxide−Resin Nanocomposites of Tunable Structure for Arsenite Removal: Effect of the Host Pore Structure. *J. Hazard. Mater.* **2011**, *198*, 241−246.
(41) Liu, H.; Sun, X. F.; Yin, C. Q.; Hu, C. Removal of Phosphate by Mesoporous ZrO_2. *J. Hazard. Mater.* **2008**, *151*, 616−622.
(42) Burleson, D. J.; Penn, R. L. Two-Step Growth of Goethite from Ferrihydrite. *Langmuir* **2006**, *22*, 402−409.

DOI: 10.1021/acsami.5b06098
ACS Appl. Mater. Interfaces 2015, 7, 20835−20844